Journal of Materials Chemistry A

Non-Confined Gamma Monoclinic Sulfur Cathode in Carbonate Electrolyte Based Room Temperature K-S Batteries

Journal:	*Journal of Materials Chemistry A*
Manuscript ID	TA-ART-03-2023-001751.R2
Article Type:	Paper
Date Submitted by the Author:	08-Jun-2023
Complete List of Authors:	Pai, Rahul; Drexel University College of Engineering, Chemical and Biological Engineering Cardoza, Neal; Drexel University College of Engineering, Chemical and Biological Engineering Natu, Varun ; Drexel University, Department of Materials Science and Engineering Barsoum, Michel; Drexel University, Department of Materials Science and Engineering Kalra, Vibha; Drexel University, Chemical and Biologial Engineering

ARTICLE

Non-Confined Gamma Monoclinic Sulfur Cathode in Carbonate Electrolyte Based Room Temperature K-S Batteries

Received 00th January 20xx,
Accepted 00th January 20xx

DOI: 10.1039/x0xx00000x

Rahul Pai[a], Neal Amadeus Cardoza[a], Varun Natu[c], , Michel W. Barsoum[b], Vibha Kalra[a,*]

Potassium-sulfur cells have garnered a lot of interest as a grid storage chemistry due to the high abundance of both elements and hence their low cost. However, their development is hindered by the polysulfide shuttle effect and their dependency on electrolytes with limited commercial viability. The inability to use carbonate electrolytes is due to the irreversible reaction between it and PS, rendering the cell useless in the first few cycles. Here we expand our use of monoclinic γ-sulfur in carbon nanofibers (γS-CNFs) to the potassium-sulfur, K-S, chemistry. Herein we show that using γ-S enables the cells to run for 500 cycles at ~900 mAh.g^{-1} in commercial carbonate electrolytes. We further attempt to understand the role of γS-CNFs in K-S cells with electrochemical characterization and postmortem spectroscopy. As far as we are aware this is the first application of γ-S in K-S cells. Its outstanding performance should lead to new avenues for the development of this promising chemistry.

Introduction

Currently, lithium-ion batteries, LIB, are the dominant players in the battery domain and find their applications in a huge variety of fields ranging from portable electronics to medical devices.[1–3] However, the increasing demand for energy from emerging applications such as all-electric vehicles requires battery chemistries with lower cost and significantly longer cycle life.[4–6] Room temperature, RT, metal sodium, potassium, magnesium, and alumninum (Na/K/Mg/Al)-S batteries have attracted extensive interest due to their higher theoretical capacities (1675 mAh.g^{-1} for K), increased abundancy compared to Li rendering them both cheaper and more environmentally benign.[7,8,9,10,11–13] Amongst them, potassium-sulfur (K-S) batteries have a similar potential compared with Li . (-2.93 V for K/K$^+$, -3.05 V for Li/Li$^+$, and -2.71 V for Na/Na$^+$ vs SHE).[14,15] Furthermore, it is reported, that K ion electrolytes possess relatively higher conductivities than Li$^+$ due to the weaker Lewis acidity of K and the resultant smaller stokes radius of solvated K$^+$ ion than lithium.[16–18]

K-S batteries share similar reaction mechanisms with their Li-S counterparts. However, they exhibit more aggravated problems pertaining to reversibility and capacity fade due to their higher reactivity with polysulfides, PS, leading to loss of cathodic active material.[19–21] Furthermore, the higher ionic radius of K$^+$ ions and poor conductivity of S causes sluggish reaction kinetics leading to an incomplete reduction of S (to K_2S_4/K_2S_3 vs. K_2S_2/K_2S) resulting in lower accessible capacity.[19–21] Like Li-S, the electrolyte of choice has been ether electrolytes, as the soluble PS of both Li and K will react with carbonate electrolytes.[22] However, this is not ideal as ether electrolytes suffer from a low flash point (42°C) compared to the commercial carbonate-based electrolytes (BP >220°C). K PSs and Na PSs have reduced solubility in carbonate electrolytes compared with Li PSs. It has been theorized the larger ionic radius of K$^+$ and Na$^+$ compared to Li$^+$ renders the K$^+$ PS ion less dissociated in polar solvents.[23] This property enables the use of carbonate electrolytes with little S confinement in comparison to Li-S.

Various mitigation approaches have been utilized to reduce the level of polysulfide dissolution and improve conversion in K-S cells.[24] Catalysts such as 1-methylimidazole solvated Cu have been shown to improve the conversion of K PSs leading to a high reversible capacity of 922 mAh.g^{-1}.[25] Chen et al. showed that coating a mesoporous C infiltrated with S with a polyaniline coating resulted in 329.3 mAh g^{-1} after 50 cycles at 50 mA g^{-1}.[20] However, these approaches do not allow for the use of commercial carbonate electrolytes due to the adverse reactions with polysulfides.

There are two main methods that have been implemented to use commercial carbonate electrolytes. Chemically bound S is the first strategy which is made by heating S and polyacrylonitrile demonstrated by Wang et. al.[26] This material has since been used multiple times in Li-S and K-S batteries with carbonate electrolyte.[26–28] This approach however results in limited S loading and higher impedance from the polymeric backbone. Another approach to improve S-utilization, conversion, and capacity retention, is to confine S in microporous C. The small S molecules (S_{2-4}) confined in the microporous C greatly reduces the formation of PSs via direct conversion of the S to K_2S that results in faster conversion and more capacity retention. The fact that that these systems can use commercially-viable carbonate

[a] Department of Chemical and Biological Engineering, Drexel University, 3141 Chestnut Street, Philadelphia, PA-19104.
[b] Department of Material Science Engineering, Drexel University, 3141 Chestnut Street, Philadelphia, PA-19104
[c] Physical and Materials Chemistry Division, CSIR-National Chemical Laboratory, Pune, 411008 Maharashtra, India
*Corresponding author: vk99@drexel.edu
† Footnotes relating to the title and/or authors should appear here.
Electronic Supplementary Information (ESI) available: [details of any supplementary information available should be included here]. See DOI: 10.1039/x0xx00000x

electrolytes is an added bonus.[29–31] This comment notwithstanding, the papers on this microporous confined S are a small fraction of current research in K-S batteries.

The main disadvantages of confinement strategies is the need to develop ultra-microporous C (< 0.7 nm) that require a complex, multi-step, processes of pore formation at temperatures greater than 500 °C. [29–32] Moreover, to the best of our knowledge, there are no reports where the S is unconfined in K-S batteries with a carbonate electrolyte.

In this study, we extend our novel γ-S phase approach to the K-S chemistry.[33] We demonstrate that despite S being in an un-confined state in our host C material, in this case, C nanofibers (CNFs), we achieve reversible capacity in presence of a carbonate electrolyte in K-S batteries. In this work, we demonstrate successful operation of our cathode in carbonate electrolyte by utilizing a monoclinic polymorph of S in an unconfined state, thereby, suggesting the possibility of direct solid conversion eliminating the formation of soluble PS. We hypothesize the functioning of the S in a non-confined state can be attributed to the structural orientation of the monoclinic phase. We shed light on the crystal structure formed on the CNF architecture and understand the reaction mechanism via post-mortem spectroscopy. The cathode delivers a stable capacity of 925 mAh.g^{-1} after the first two cycles and remains stable for 500 cycles at a current rate of 0.1C. We show through postmortem XPS evidence for the formation of K_2S.

Experimental

Synthesis of C nanofibers (CNFs)

Here we use the same method we used previously to fabricate free-standing CNFs mats.[33] In short, a solution of dimethylformamide (DMF, 99.9% purity) with 10 wt.% polyacrylonitrile (PAN, Mw 150 000 g mol^{-1}) is stirred until the polymer dissolves. The solution is then poured into a syringe (Becton Dickinson 5 mL) with an 18-gauge stainless steel Luer Lock tip (Hamilton Corp., Reno, Nevada). The solution filled syringe is loaded into a NE-400 pump system (New Era Pump Systems, Inc.), to control the feed rate to 0.2 ml.h^{-1} of solution. The combination is placed into an inhouse-built chamber that controls the relative humidity to < 15%. The distance between the grounded aluminum, Al, fiber collector and the needle tip is 6 inches. The needle tip is charged to 7-8kV using a Series ES -30 kV power supply (Gamma High Voltage Research, Inc.). The fiber mat was peeled off the Al collector, transferred on to an alumina plate and heated in air to 280°C for 6 h. After, which the nanofiber mat is carbonized at 900°C tube furnace (MTI, Corp.) under N_2 flow. At 900°C for 1 h, the N_2 gas is replaced be CO_2. After which the CNFs mat is then cooled to room temperature and then used for S deposition.

Monoclinic γ-Sulfur C Nanofiber (γS-CNFs) synthesis

Sulfur (sublimed, ~100 mesh, purity 99.5% trace metals basis, Alfa Aesar, USA) was loaded on the CNF mat and placed in an in house-designed autoclave. Before placing it in the autoclave the CNF mats were punched into electrodes 11 mm in diameter weighing ~ 1mg, and dried at 140°C overnight. The autoclave is made from 316 stainless steel with a reservoir of S at the bottom and a perforated stainless-steel disk was floated on a ledge above. It is on this disk that the CNFs electrode were placed, and the autoclave sealed. The autoclave was then heated to 180°C for 24 h in an oven, after which it was cooled in 12 h back to RT. The electrode weight before and after treatments were used to obtain the weight of the S in the electrode, with an average weight of 1 mg.cm^{-2}. The γS-CNFs was used as is in the cell without further modification.

Material characterization

Characterization of the CNFs and γS-CNFs was done with a Zeiss Supra VP50 field emission scanning electron microscope, SEM, with an in-lens detector and Oxford UltiMax 40mm energy dispersive spectrometer, EDS. X-ray diffraction, XRD, patterns were carried out on a Rigaku Smartlab, with Cu Kα radiation (40 kV and 44 mA). The step size was 0.02° and dwell time of 5 sec. X-ray photo spectroscopy, XPS, of the cathodes were done with a spot size of 200 µm, pass energy of 23.5 eV using a Physical Electronics Versa Probe 5000 with monochromatic Al Kα as the excitation source. The XPS data was processed on the CasaXPS software. A TA instrument 2950 was used for thermogravimetric analysis, TGA, with an argon flow of 40 ml.min^{-1} and heating rate of 10°C.min^{-1}. Porosity of the CNFs and γS-CNFs were carried out on an AutoSorb iQ2 automated gas sorption analyzer from Quantachrome Instruments, at -196.15°C, after degassing at 150°C under N_2 flow.

Electrochemical characterization

Coin cells were built using standard 2032 cell parts (MTI and Xiamen TMAX battery equipment) for electrochemical characterization. Cells were assembled inside an argon, Ar, glovebox (Mbraun Labstar Pro, H_2O and O_2 less than 1 ppm). The cathodes with ~1 mg.cm^{-1} of S were dried under vacuum in the antechamber overnight before being brought into the glovebox. The CR2032 cells were assembled with a 19 mm Celgard 2325, potassium, K, anode 15.6 mm (cut from a rod,

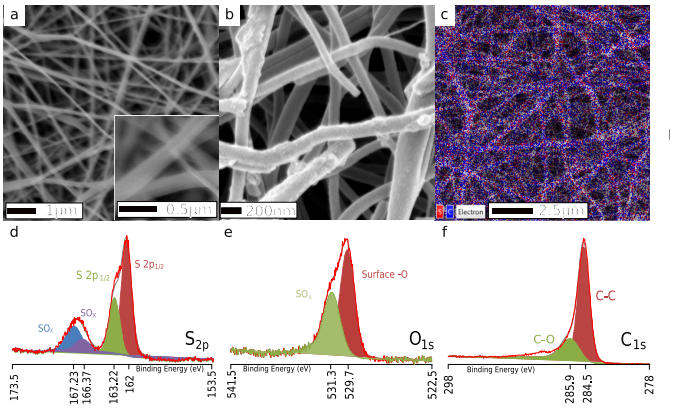

Figure 1 a) SEM images of CNFs that were activated via CO_2 before γ-S deposition, b) after γ-S deposition (γS-CNFs), c) EDS of γS-CNFs C distribution additional EDS data can be seen in figure S1, d) S distribution, e) XPS measurements of the γS-CNFs of the γS-CNFs of S 2p, f) oxygen 1s, g) C 1s, additional XPS data can be seen in figure S3

Alfa Aesar), a stainless-steel spacer and a stainless-steel spring (MTI and Xiamen TMAX battery equipment). The electrolyte was added according to a E/S of 20µL to 1mg of S. Electrolyte used here was 1M of potassium hexafluorophosphate (KPF_6) with equal volumes of battery grade ethylene carbonate, diethyl carbonate (EC:DEC 1:1) (EC, purity ≥ 99%, acid < 10 ppm, H_2O < 10 ppm) (DEC, purity ≥ 99%, acid < 10 ppm, H_2O < 10 ppm). The solvents were dried over molecular sieves before being used. All the electrolyte components were purchased from Sigma Aldrich. The cells were then crimped in an automatic hydraulic crimper (MTI) and used as is for experiments. Potentiostatic experiments were run on a VMP3 (Biologic) between 0.1-3V vs K/K^+, using 0.1-1 $mV.s^{-1}$ for scan rates. Galvanostatic experiments were run on Neware BTS 4000 series and Maccor 4000 series, at various c-rates with 1C being 1675 $mA.g^{-1}$.

Results and discussion

The (γS-CNFs) that emerges from the autoclave was characterized to understand the material better Figure 1a and 1b shows SEM images of CNFs before and after S deposition. The post S deposition CNFs display a rough fiber morphology, that reveals consistent and conformal S deposition on the surface as well as some deposition within the interfiber spacing. Furthermore, the S deposition technique retains the CNF architecture with no aggregates of CNFs or structural collapse. EDS shows the presence of uniformly distributed S in the composite, as shown in Figure 1c. Separate images of EDS elements are shown in Figure S1. To further understand the nature of the crystal structure of the sulfur-based CNFs, XRD analysis was conducted. Figure S2 shows XRD patterns of CNFs before and after S deposition. The CNFs before thermal treatment show no significant diffraction peaks. A wide hump is seen around of 20-30° 2θ due to the amorphous nature of C in CNFs. After the S deposition, we see a rare and metastable phase of S – the monoclinic γ phase. This is a striking behavior as monoclinic phases (beta and gamma) are understood to be stable beyond 94.4°C and below 119°C.[33] Nevertheless, repeatable XRD signatures after S deposition treatment show the presence of γ-monoclinic S in our CNFs samples at room temperature. We hypothesize the stability of γS is attributed to the structure of C in our activated CNFs host. DFT work shows that if the C atoms exceed 0.3 per S8 unit crystal structure, leads to the room temperature stabilization of monoclinic S phase.[34] We believe the activation process of heating the fibers under CO_2 atmosphere makes the surface of fibers rough which facilitates the development and stabilization of this phase in a non-confined state as predicted by the DFT study. XPS was used on γS-CNFs to validate the chemical composition and surface properties seen in Figure 1d-f. The survey spectra show the existence of C1s, S2p, and O1s peaks in the composite seen in Figure S3. The peak at 285.9 eV, 284.6 eV, 531 eV, 533 eV, 163.7 eV, and 164.9 eV can be attributed to surface oxidation of C, C for the C1s spectra, surface oxygen in O1s, surface hydroxyl group in O1s, S in the 2p3/2, and 2p1/2 respectively. The S peaks (163.7 eV, and 164.9 eV) with an area ratio of 1:2 ΔE of 1.16 eV are the characteristics of solid S in the composite.[37] Surface oxidation of S during the deposition from the elevated temperature can be seen in the peaks centered at 167.23 eV and 166.37 eV. The smooth Lorentzian asymmetric peak of the conductive C host further confirms that S does not react with the bare C surface Figure S4 shows the thermogravimetric analysis of γS-CNFs conducted in an inert Ar flow with a heating rate of 10°C/min from room temperature to 600°C. Weight loss below 100°C can be attributed with adsorbed water evaporation. After 100°C the continuous weight loss can be split into two sections with two different degradation rates. This can be explained by the γS on the CNF surface evaporating at 119°C as the first region. The S deeper in the porous activated CNFs evaporates at the higher temperature, which is still under 300°C. This indicates that while the S exists in the pores of the CNFs, the pores do not confine S. If S was truly confined via only physical confinement the vaporization temperature would be higher than 300°C.[30,38] This is not seen in the TGA for γS-CNFs. The S content in the γS-CNFs determined by TGA was ~50 wt.%. Additionally, while

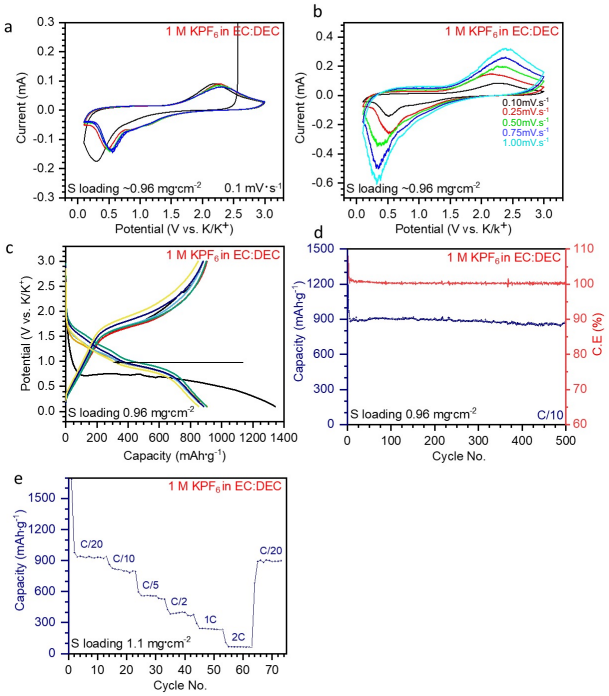

Figure 2 Electrochemical performance: a. CV, b. CV as a function of scan rate, c. Voltage profiles at various cycles numbers 1, 2,5, 10, 100, 300, 500, d. Cycling performance, e. Rate performance.

we can see S in the pores by the lack of porosity after S deposition in the pore size distribution and the N_2 isotherms in Figure S4. We also can observe S on the surface of the CNFs in Figure 1A and 1B. Also, the γS crystal structure observed via XRD, which is not shielded by C seen in Figure S2. Lastly in our prior work with γS we showed non-activated CNFs still cycle with a stable plateau and a capacity of c.a. 400 $mAh.g^{-1}$.[34] It is clear despite some S existing in the pores of the CNF it alone cannot explain the electrochemical performance in carbonate electrolytes.

To test the electrochemical response of our γS-CNFs system, coin cells were assembled with γS -CNFs as the cathode and K foils as anodes. The electrolyte employed was 1M KPF_6 in EC: DEC. Figure 2a shows cyclic voltammetry curves of γS -CNFs at a scan rate of 0.1 mV/s in a voltage range of 0.1-3.0 V vs K/K+. In the first cycle, we observe an irreversible peak at 0.3V which is then replaced by a single broad reduction peak at 0.5V vs K/K+ and a broad oxidation peak in subsequent cycles. The first irreversible reduction peak can be ascribed to the formation of solid electrolyte interphase (SEI) on the surface of the γS-CNFs electrode as well as the activation of C bonded to S. At the base of the broad reduction peak at 0.8V, we start to see the potassiation process of S. Several K-PS (K_2S_6, K_2S_5, K_2S_4, K_2S_3, K_2S_2, K_2S) are present at room temperature and the polarization gap for the formation of individual species is high.[19] This coupled with sluggish kinetics results in the need for lower voltage for complete conversion.[19] The oxidation peak at 2.26V corresponds to the formation of S and its broad nature suggests formation of different chain lengths.[19] In addition, no peaks at ~2.3V during the first reduction cycle further indicate that soluble PS species were not formed. The lack of the upper voltage peak suggests the formation solid short chain K-PS and some insoluble long chain K-PS. The longer insoluble PS can be attributed to larger ionic radius of the K ion on the PS impeding the dissolution into carbonate electrolytes.[23] In the past, it has been established that cyclo-S8 forms thiocarbonate and ethylene glycol due to the irreversible reduction reaction of PS with carbonate electrolyte species causing the batteries to fail after the first cycle.[22] Figure 2b shows the current response with changing scan rate (0.1-1 $mV.s^{-1}$) which demonstrates similar redox behavior at high scan rates. Figure 2c displays the charge-discharge curves of γS-CNFs at various cycles at a current rate of C/10. The first cycle delivers a capacity of 1350 $mAh.g^{-1}$ after which it delivers a reversible capacity of 900 $mAh.g^{-1}$. In the discharge curve, a main monotonically decreasing curve can be seen, that is related to a possible solid-solid reduction of γ-S, which stays consistent in later cycles. This can be attributed to the single plateau seen in the voltage profiles in Figure 2c, which is similar to the single plateaus obtained with S confined in microporous C in carbonate electrolytes.[30–32,39] These papers also show single plateaus, that is the direct solid to solid conversion of S to short chain PS. These papers employ chemical and physical confinement of S as the S used is α-orthorhombic. Whereas in our paper γS sits exposed on the surface of the CNFs. As there is no confinement of S with γS, yet we still observe single plateaus on the voltage curve, This behavior is also like the single plateaus with γS in Li-S.[34] The cycling curve is shown in. Figure 2d, the γS-CNFs cathode retains 96% capacity after 1st cycle. The higher than 100% coulombic efficiency in the 1st cycle can be attributed to the irreversible formation of the SEI, via the decomposition of the electrolyte as the voltage drops below 1V. The rate performance was evaluated at various current rates from C/20 to 2 C (Figure 2e). A capacity of ~950, 800, 550, 325, and 90 mAh.g-1 was achieved at C/20, C/10, C/5, C/2, 1C, and 2C, respectively. Upon further decrease in current rate (C/20) a capacity of ~900 $mAh.g^{-1}$ was achieved, indicating a good rate performance.

Table 1 lists the electrochemical performance of pore confined S in microporous C and sulfurized polymers, the competing solutions enabling the use of carbonate electrolytes. The γS-CNFs in K-S in comparison to those solutions have shown remarkable stability and capacity retention along with capacity. Such performance in carbonate electrolytes can be associated with the possible conversion of γS to lower-order K PS via a solid-state reaction which eliminates PS formation and thereby eliminating the PS shuttle effect.

To further get an insight into the development of γS and its reaction mechanism in carbonate electrolytes, crystal structure simulation, and postmortem characterizations were conducted, in both reflection and transmission modes seen in Figure 3 along with Figure S6 shows the calculated x-ray diffraction of γS along with the simulated pattern generated using CrystalMaker® (CrystalMaker Software Ltd, Oxford, England (www.crystalmaker.com)) from the crystal structure (COD: 9009801).[40–47] The simulated powder diffraction was manipulated in CrystalDiffract® (CrystalMaker Software Ltd, Oxford, England (www.crystalmaker.com)) with preferred orientation in the k-direction (010). Upon closer observation, we can see the simulated γS structure oriented in k-direction with plates geometry has peaks like the ones observed in our reflectance experimental diffraction pattern. During transmission mode the CNF was staged upright perpendicular to the surface and the x-rays pass through the sample. As CrystalDiffract® can

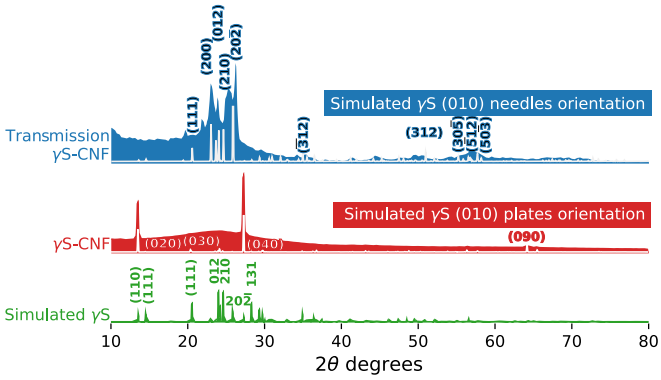

Figure 3 Simulated and experimental XRD patterns of γS and γS-CNFs. Simulated patterns in preferred k-direction (010) orientation shown in white overlayed on experimental data shown in solid blue and red. Normal reflectance XRD matches simulated γS in the plate geometry orientation in the 010 direction. Transmission XRD best matches the same 010 direction but with needle geometry, as the needle geometry emulates the transmission mode of the plate geometry. Simulated γS at the bottom has no orientation. More peak hkl details can be seen in figure S6.

only simulate reflectance mode data, setting the orientation to needle geometry emulates the transmission mode, From the perspectives of the x-rays during transmission mode the surface would look like needle growth which are just plates turned 90°. This preferentially oriented γS structure in the k-direction results in a ladder like structure at the molecular level seen in Figure 4. We hypothesis the k-directionality of the γS allows for K^+ to intercalate through the structure. To better understand the reaction mechanism between S and K during redox reactions, in

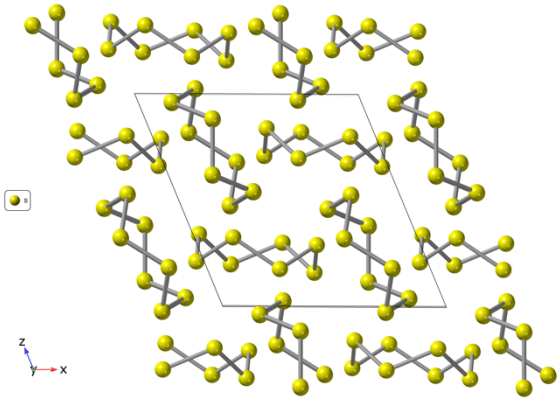

Figure 4 Ladder structure for k-direction of γS generated from COD:9009801 [30–37]

this work, postmortem XPS analysis was conducted on electrodes held at different potentials. To get an understanding of the surface species of the electrodes at various voltages during discharge and charge cycles, XPS analysis was carried out seen in Figure 5 The pristine electrode in the S2p spectra shows the presence of S doublet peaks (S 2p3/2 and S 2p1/2) positioned at 163.7 and 164.9 eV with a peak separation of 1.16 eV.[36] In addition, we see a peak at higher binding energy (168.94 eV) associated with the formation of surface oxides during high-temperature S deposition. As we discharge the electrode to 1.5V, we see changes in the S2p region. We observe a multitude of peaks with dominant species in each discharge and charge voltages. As we reduce the γS, we observe the formation of higher-order K-PS (K_2S_6/K_2S_4) which later are reduced to K_2S_2 and K_2S as we further discharge it to 0.1V. We observe the K_2S peak at energies <160 eV.[27] Upon charging we observe a complete reversal of products formed on discharge as the K_2S shoulder intensity decreases. Coinciding with the increase of the PS K_2S_4 and K_2S_3. At the end of the charge cycle those PS peaks then shift to predominantly S2p1/2 and S2p3/2. Indicating the transformation back to S is nearly complete. During reduction reaction, the K_2S_2 phase was not observed in XPS results and this can be associated with the higher formation energy compared to K_2S_3 and K_2S.[48,49] This postmortem study demonstrates the complete conversion of γS to K_2S. This allows for higher S utilization and stable cycling as active material is not lost to K_2S. Further work with this unique phase is needed in future studies, particularly modelling to better understand the mechanism of this phase in the K-S chemistry.

Conclusions

This work extends our novel approach of polysulfide (PS) mitigation to the K-S chemistry, enabling extremely stable cycling to 500 cycles in carbonate electrolyte. The use of carbonate electrolyte in the metal-S chemistry has long since been a challenge, due to polysulfide irreversible interactions with it. Existing strategies like small molecule S confinement have a loading limitation among other issues. In this work we leverage the novel γS phase to use carbonate electrolyte. The developed unique monoclinic gamma phase on CNFs has preferential orientation in k-direction which might be possibly contributing to single-step conversion and its stability at room temperature. This leads to extremely stable cycling for 500 cycles at ~ 900 $mAh.g^{-1}$ in carbonate electrolyte. Postmortem XRD and XPS analysis further disseminate the possible redox products after charge-discharge processes. This demonstrated complete conversion to K_2S and conversion back to S. Further modelling work to better understand the mechanism of the γS and the role of C in its stabilization is needed. Additionally, in-situ and in-operando work would be beneficial in elucidating the mechanism of γS. The development of unconfined S cathodes in K-S batteries employing carbonate-based electrolytes can revolutionize the field of mass production of commercial batteries.

Conflicts of interest

V.K. and R.P. are co-inventors on patent US20200321600A1. All other authors declare no competing interests.

Acknowledgements

Authors would like to thank the Drexel Ventures Innovations Fund, the National Science Foundation (CMMI-1804374) for funding, and the Drexel Material Characterization Core (RRID:SCR_022684).

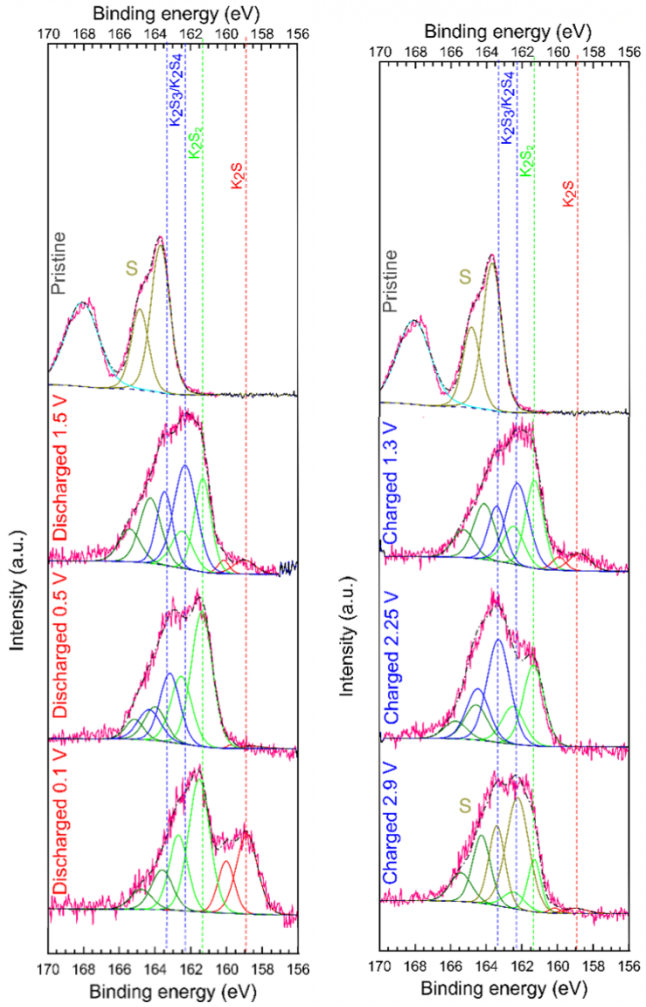

Figure 5 Postmortem XPS analysis of samples as a function of voltages during discharge and charge cycles, showing the PS pathways with the γS in a K-S cell.

Table 1 Comparison of electrochemical performance with other carbonate strategies for K-S cells

Cathode	Electrolyte	S content (wt.%)	S loading (mg.cm^{-2})	Capacity (mAh.g$_S^{-1}$)	Rate	Capacity retention (%) at (Cycles)	Voltage Window (V)	Ref
Sulfurized polyacrylonitrile	0.5 M KPF_6 EC:DMC	36	1.5	708	0.5C	69.8 at 100 cy	0.1-3.0	27
Microporous C	0.8 M KPF_6 EC:DEC	20	0.5-1	870	20 mA.g^{-1}	73 at 150 cy	0.5-3.0	30
Microporous C	0.8 M KPF_6 EC:DEC	37.8	1.5-2.0	826	0.2C	69.9 at 50 cy	0.5-3.0	31
Gamma sulfur (γS-CNFs)	1M KPF_6 EC:DEC	50	0.96	900	0.1C	95 at 500 cy	0.1-3.0	This work

Notes and references

1 M. Armand and J.-M. Tarascon, Building better batteries, *Nature*, 2008, **451**, 652–657.
2 C. P. Grey and D. S. Hall, Prospects for lithium-ion batteries and beyond—a 2030 vision, *Nat Commun*, 2020, **11**, 6279.
3 M. Li, J. Lu, Z. Chen and K. Amine, 30 Years of Lithium-Ion Batteries, *Adv. Mater.*, 2018, **30**, 1800561.
4 D. L. Wood, J. Li and C. Daniel, Prospects for reducing the processing cost of lithium ion batteries, *Journal of Power Sources*, 2015, **275**, 234–242.
5 United States Advanced Battery Consortium, *Advanced Batteries for Electric Vehicles - 2020 Commercialization Goals*, U.S.A.B.C, Southfield, MI 48075, 2015.

6 F. Wu, J. Maier and Y. Yu, Guidelines and trends for next-generation rechargeable lithium and lithium-ion batteries, *Chem. Soc. Rev.*, 2020, **49**, 1569–1614.
7 Y. Li, Y. Zeng, Y. Chen, D. Luan, S. Gao and X. W. Lou, Mesoporous N-rich Carbon with Single-Ni Atoms as a Multifunctional Sulfur Host for Li-S Batteries, *Angewandte Chemie International Edition*, 2022, **61**, e202212680.
8 F. Shi, J. Yu, C. Chen, S. P. Lau, W. Lv and Z.-L. Xu, Advances in understanding and regulation of sulfur conversion processes in metal–sulfur batteries, *J. Mater. Chem. A*, 2022, **10**, 19412–19443.
9 Z. Li, J. T. Zhang, Y. M. Chen, J. Li and X. W. Lou, Pie-like electrode design for high-energy density lithium–sulfur batteries, *Nat Commun*, 2015, **6**, 8850.
10 J. Zhang, Z. Li, Y. Chen, S. Gao and X. W. Lou, Nickel–Iron Layered Double Hydroxide Hollow Polyhedrons as a Superior Sulfur Host for Lithium–Sulfur Batteries, *Angewandte Chemie International Edition*, 2018, **57**, 10944–10948.
11 A. Manthiram, Y. Fu, S.-H. Chung, C. Zu and Y.-S. Su, Rechargeable Lithium–Sulfur Batteries, *Chemical Reviews*, 2014, **114**, 11751–11787.
12 Y.-X. Yin, S. Xin, Y.-G. Guo and L.-J. Wan, Lithium-Sulfur Batteries: Electrochemistry, Materials, and Prospects, *Angew. Chem. Int. Ed.*, 2013, **52**, 13186–13200.
13 A. Manthiram and X. Yu, Ambient Temperature Sodium-Sulfur Batteries, *Small*, 2015, **11**, 2108–2114.
14 A. Eftekhari, Z. Jian and X. Ji, Potassium Secondary Batteries, *ACS Appl. Mater. Interfaces*, 2017, **9**, 4404–4419.
15 A. Eftekhari, The rise of lithium–selenium batteries, *Sustainable Energy Fuels*, 2017, **1**, 14–29.
16 Y. Liu, C. Gao, L. Dai, Q. Deng, L. Wang, J. Luo, S. Liu and N. Hu, The Features and Progress of Electrolyte for Potassium Ion Batteries, *Small*, 2020, **16**, 2004096.
17 G. G. Eshetu, G. A. Elia, M. Armand, M. Forsyth, S. Komaba, T. Rojo and S. Passerini, Electrolytes and Interphases in Sodium-Based Rechargeable Batteries: Recent Advances and Perspectives, *Advanced Energy Materials*, *Adv. Energy Mater.* 2020, **10**, 2000093.
18 M. Okoshi, Y. Yamada, S. Komaba, A. Yamada and H. Nakai, Theoretical Analysis of Interactions between Potassium Ions and Organic Electrolyte Solvents: A Comparison with Lithium, Sodium, and Magnesium Ions, *J. Electrochem. Soc.*, 2017, **164**, A54–A60.
19 X. Zhao, Y. Lu, Z. Qian, R. Wang and Z. Guo, Potassium-sulfur batteries: Status and perspectives, *EcoMat*, 2020, **2**, e12038.
20 Q. Zhao, Y. Hu, K. Zhang and J. Chen, Potassium–Sulfur Batteries: A New Member of Room-Temperature Rechargeable Metal–Sulfur Batteries, *Inorg. Chem.*, 2014, **53**, 9000–9005.
21 J. Ding, H. Zhang, W. Fan, C. Zhong, W. Hu and D. Mitlin, Review of Emerging Potassium–Sulfur Batteries, *Advanced Materials*, 2020, **32**, 1908007.
22 T. Yim, M.-S. Park, J.-S. Yu, K. J. Kim, K. Y. Im, J.-H. Kim, G. Jeong, Y. N. Jo, S.-G. Woo, K. S. Kang, I. Lee and Y.-J. Kim, Effect of chemical reactivity of polysulfide toward carbonate-based electrolyte on the electrochemical performance of Li–S batteries, *Electrochimica Acta*, 2013, **107**, 454–460.
23 Y. Wang, D. Zhou, V. Palomares, D. Shanmukaraj, B. Sun, X. Tang, C. Wang, M. Armand, T. Rojo and G. Wang, Revitalising sodium–sulfur batteries for non-high-temperature operation: a crucial review, *Energy & Environmental Science*, 2020, **13**, 3848–3879.
24 W. Zhang, Y. Liu and Z. Guo, Approaching high-performance potassium-ion batteries via advanced design strategies and engineering, *Sci. Adv.*, 2019, **5**, eaav7412.
25 N.-C. Lai, G. Cong and Y.-C. Lu, A high-energy potassium–sulfur battery enabled by facile and effective imidazole-solvated copper catalysts, *J. Mater. Chem. A*, 2019, **7**, 20584–20589.
26 J. Wang, J. Yang, C. Wan, K. Du, J. Xie and N. Xu, Sulfur Composite Cathode Materials for Rechargeable Lithium Batteries, *Advanced Functional Materials*, 2003, **13**, 487–492.
27 J.-Y. Hwang, H. M. Kim and Y.-K. Sun, High performance potassium–sulfur batteries based on a sulfurized polyacrylonitrile cathode and polyacrylic acid binder, *J. Mater. Chem. A*, 2018, **6**, 14587–14593.
28 S. Wei, L. Ma, K. E. Hendrickson, Z. Tu and L. A. Archer, Metal–Sulfur Battery Cathodes Based on PAN–Sulfur Composites, *J. Am. Chem. Soc.*, 2015, **137**, 12143–12152.
29 G.-B. Cho, H.-B. Park, J.-S. Jeong, M.-R. Chae, Y.-M. Im, L. Han-Gyeol, P. Sang-Hui and K.-W. Kim, Effect of Ball Milling on Electrochemical Properties of Sulfur/Polyacrylonitrile (SPAN) Cathode in Li/S Battery, *Journal of Nanoscience and Nanotechnology*, 2018, **18**, 6431–6436.
30 P. Xiong, X. Han, X. Zhao, P. Bai, Y. Liu, J. Sun and Y. Xu, Room-Temperature Potassium–Sulfur Batteries Enabled by Microporous Carbon Stabilized Small-Molecule Sulfur Cathodes, *ACS Nano*, 2019, **13(2)**, 2536-2543.
31 L. Hu, X. Meng, L. Liu, D. Liang, S. Liang, L.-L. Wang, L. Yang, T. Ding, C. Deng and Q. Dong, A superficial sulfur interfacial control strategy for the fabrication of a sulfur/carbon composite for potassium–sulfur batteries, *Chem. Commun.*, 2021, **57**, 1490–1493.
32 R. Ma, L. Fan, J. Wang and B. Lu, Confined and covalent sulfur for stable room temperature potassium-sulfur battery, *Electrochimica Acta*, 2019, **293**, 191–198.
33 A. D. Dysart, N. A. Cardoza, G. Mitchell, V. Ortalan and V. G. Pol, Effect of Synthesis Method Using Varying Types of Micropore Level Sulfur Infiltration on Electrochemical Performance in Lithium–Sulfur Batteries, *Energy Technol.*, 2019, **7**, 1900194.
34 R. Pai, A. Singh, M. H. Tang and V. Kalra, Stabilization of gamma sulfur at room temperature to enable the use of carbonate electrolyte in Li-S batteries, *Commun Chem*, 2022, **5**, 1–11.
35 S. C. Jung and Y.-K. Han, Monoclinic sulfur cathode utilizing carbon for high-performance lithium–sulfur batteries, *Journal of Power Sources*, 2016, **325**, 495–500.
36 C. Powell, 1989.
37 X. Liang, C. Hart, Q. Pang, A. Garsuch, T. Weiss and L. F. Nazar, A highly efficient polysulfide mediator for lithium–sulfur batteries, *Nat Commun*, 2015, **6**, 5682.
38 Z. Li, L. Yuan, Z. Yi, Y. Sun, Y. Liu, Y. Jiang, Y. Shen, Y. Xin, Z. Zhang and Y. Huang, Insight into the Electrode Mechanism in Lithium-Sulfur Batteries with Ordered Microporous Carbon Confined Sulfur as the Cathode, *Adv. Energy Mater.*, 2014, **4**, 1301473.
39 B. Zhang, C. Lai, Z. Zhou and X. P. Gao, Preparation and electrochemical properties of sulfur–acetylene black composites as cathode materials, *Electrochimica Acta*, 2009, **54**, 3708–3713.
40 S. Moon, Y. H. Jung, W. K. Jung, D. S. Jung, J. W. Choi and D. K. Kim, Encapsulated Monoclinic Sulfur for Stable Cycling of Li-S Rechargeable Batteries, *Adv. Mater.*, 2013, **25**, 6547–6553.
41 T. Kr□uter and B. Neum□ller, Reaktionen von Diorganogallium(indium)fluoriden. Die Kristallstruktur von Mes2InF, *Z. Anorg. Allg. Chem.*, 1995, **621**, 597–606.

42 A. Vaitkus, A. Merkys and S. Gražulis, Validation of the Crystallography Open Database using the Crystallographic Information Framework, *J Appl Crystallogr*, 2021, **54**, 661–672.
43 M. Quirós, S. Gražulis, S. Girdzijauskaitė, A. Merkys and A. Vaitkus, Using SMILES strings for the description of chemical connectivity in the Crystallography Open Database, *J Cheminform*, 2018, **10**, 23.
44 A. Merkys, A. Vaitkus, J. Butkus, M. Okulič-Kazarinas, V. Kairys and S. Gražulis, *COD::CIF::Parser* : an error-correcting CIF parser for the Perl language, *J Appl Crystallogr*, 2016, **49**, 292–301.
45 S. Gražulis, A. Merkys, A. Vaitkus and M. Okulič-Kazarinas, Computing stoichiometric molecular composition from crystal structures, *J Appl Crystallogr*, 2015, **48**, 85–91.
46 S. Gražulis, A. Daškevič, A. Merkys, D. Chateigner, L. Lutterotti, M. Quirós, N. R. Serebryanaya, P. Moeck, R. T. Downs and A. Le Bail, Crystallography Open Database (COD): an open-access collection of crystal structures and platform for world-wide collaboration, *Nucleic Acids Research*, 2012, **40**, D420–D427.
47 S. Gražulis, D. Chateigner, R. T. Downs, A. F. T. Yokochi, M. Quirós, L. Lutterotti, E. Manakova, J. Butkus, P. Moeck and A. Le Bail, Crystallography Open Database – an open-access collection of crystal structures, *J Appl Crystallogr*, 2009, **42**, 726–729.
48 S. Gu, N. Xiao, F. Wu, Y. Bai, C. Wu and Y. Wu, Chemical Synthesis of K_2S_2 and K_2S_3 for Probing Electrochemical Mechanisms in K–S Batteries, *ACS Energy Lett.*, 2018, **3**, 2858–2864.
49 C. Ye, J. Shan, D. Chao, P. Liang, Y. Jiao, J. Hao, Q. Gu, K. Davey, H. Wang and S.-Z. Qiao, Catalytic Oxidation of K_2S via Atomic Co and Pyridinic N Synergy in Potassium–Sulfur Batteries, *J. Am. Chem. Soc.*, 2021, **143**, 16902–16907.